

# Evaluation of aero-optical distortion effects in PIV

by

G.E. Elsinga<sup>(1)</sup>, B.W. van Oudheusden<sup>(2)</sup> and F. Scarano<sup>(3)</sup>

Delft University of Technology  
Department of Aerospace Engineering  
PO Box 5058, 2600 GB Delft; The Netherlands

<sup>(1)</sup>E-Mail: [g.e.elsinga@lr.tudelft.nl](mailto:g.e.elsinga@lr.tudelft.nl)

<sup>(2)</sup>E-Mail: [b.w.vanoudheusden@lr.tudelft.nl](mailto:b.w.vanoudheusden@lr.tudelft.nl)

<sup>(3)</sup>E-Mail: [f.scarano@lr.tudelft.nl](mailto:f.scarano@lr.tudelft.nl)

## ABSTRACT

Aero-optical distortion effects on velocimetry techniques, such as PTV and PIV, are investigated, which occur when the illuminated particles are observed through an optically inhomogeneous medium (e.g. compressible flows or thermal convection flows). The resulting image of the particle image pattern is subjected to deformation and blur, and in relation to particle imaging velocimetry three forms of error can be identified: position error, velocity error and particle image blur. In this paper a model is presented that describes these errors in relation to the refractive index field of the flow. The position error and the velocity error are directly related to the overall systematic error on the velocity measurement and are caused by the gradient and the second derivative of the refractive index respectively. As will be demonstrated the velocity error becomes increasingly important in large-scale PIV application to compressible flows. The particle image blur, which is related to the second derivative of the refractive index, introduces a correlation peak broadening with consequent drop in the signal to noise ratio. It is shown that particle image blur indicates that the velocity error is not negligible. Furthermore the *background oriented schlieren* technique (BOS) is proposed as a correction technique for the position and velocity error in case of 2D flows or flows with axial symmetry.

The models describing the optical distortion and the BOS correction method have been evaluated both by a computer simulation and real experiments. In the simulation two types of flow are considered: one with optical distortion normal to the flow velocity (shear layer) and one with optical distortion in the direction of the flow velocity (one-dimensional expansion). The PIV and BOS image distortion is obtained from a light ray trace through the refractive index field. These two simple flows are representative of the shear layer and Prandtl-Meyer expansion fan considered in the wind tunnel experiments. Both simulation and experiments demonstrate that the second derivative of the refractive index in the direction of the velocity vector is the major source for the velocity error. The position error is generally small and difficult to appreciate on a scale of the complete field of view. Moreover it is concluded that investigating shearing interfaces is much less critical in comparison with compression/expansion fronts. Based on the results from the simulated experiments, it is concluded that the BOS correction can reduce the velocity error up to 95%.

## 1. INTRODUCTION

Planar velocimetry techniques are nowadays applicable to low-speed flows as well as to high-speed flows including the supersonic flow regime thanks to the advances high energy pulsed lasers and CCD technology (micro-second inter-frame time). However since the first applications (Raffel and Kost 1998) the problem of applying optically based techniques through inhomogeneous media was raised. More recent applications in the supersonic regime (Urban and Mungal 2001, Haertig et al. 2002, Scarano and Van Oudheusden 2003), pointed out more clearly that the process of particle imaging in compressible flows can be far from trivial across shock waves and shear layers.

The present study investigates the aero-optical distortion effects on the accuracy of optical flow velocimetry techniques. In particular planar particle imaging techniques, such as PTV and PIV, are regarded. These methods track

the particle image motion in a planar domain within the flow field. Isolated particle images are tracked when the PTV method is followed, alternatively, the PIV technique tracks the motion of the particle image pattern within an interrogation window. Optical distortion of the imaging process occurs if the illuminated particles are observed through an optically inhomogeneous medium, as in the case of compressible flows or thermal convection flows. The resulting image of the particle image pattern is subjected to deformation and blur, and in relation to particle imaging velocimetry three forms of error are identified: position error, velocity error and particle image blur.

The position and velocity error are a direct consequence of the geometrical deformation of the image, which results in a systematic (bias) error of the velocity measurement. In synthesis one may say that the wrong velocity vector is evaluated at the wrong position. Image blur affects the tracking precision in terms of cross-correlation accuracy due to the (anisotropic) increase of the particle image size and thus correlation peak width. In the following discussion, the emphasis is given to the study of the first two types of errors. The image distortion is put in relation to the refractive index spatial distribution. From this optical model, the analytical expression of the position error is derived. Furthermore the velocity error is obtained from spatial differentiation of the position error. The effect of the scale-up of a compressible flow experiment on the optical distortion is also briefly discussed. In order to separate the effects of different sources of error, the present model assumes ideal imaging and tracking conditions, i.e. pixelization effects are neglected and the time separation between exposures is small enough to neglect the time averaging error on the velocity. Furthermore, the averaging effect of the finite interrogation window size is neglected as well. In the analysis the velocity considered is that of the particle, keeping in mind that this may differ from the flow velocity due to particle lag.

The evolution of computer-based image processing techniques allows nowadays the direct quantitative analysis of the refractive index field by either conventional Calibrated Color Schlieren or Background Oriented Schlieren techniques (CCS and BOS, Elsinga et al. 2004). The operating principle of the BOS method relies on optical distortion of a background pattern to measure the refractive index field and is therefore of direct relevance to the present problem. In addition the experimental BOS setup is very similar to that used in PIV. Therefore BOS principles can be used to describe the optical distortion effects in PTV and PIV, where a particle pattern is distorted due to the presence of a refractive index field. As will be shown, BOS can also be used to correct for the position and velocity errors in case of a 2D flow.

The model describing the optical distortion and the BOS correction method are assessed in the present investigation by means of a computer simulation (ray tracing) and a real wind-tunnel experiment. In the simulation two types of flow are considered: one with optical distortion normal to the flow velocity (shear layer) and one with optical distortion in the direction of the flow velocity (one-dimensional expansion). The PIV and BOS image distortion is obtained from a light ray trace through the refractive index field. These two simple flows are representative of the shear layer and Prandtl-Meyer expansion fan considered in the wind tunnel experiments, and which are typical basic flow features in compressible flow.

## 2. OPTICAL DISTORTION IN PIV

In this section, the error introduced in PIV by optical distortion is studied using a geometrical optics model. The position and velocity error are assessed in relation to the refractive index field between the PIV measurement plane and the imaging optics. Finally an example of particle image blur is presented.

It is assumed that the flow is steady; hence the particle velocity  $\vec{V}_p$  and the image distortion, which is related to the flow density field, depend only on the spatial location in the imaging plane. The particle-image tracking information is assumed to be sufficiently dense (high number density) to allow the measurement of the velocity spatial distribution in a continuous fashion over the field of view.

Because of the one-to-one relation between the recording plane and the plane of focus, the recorded PIV image can be thought of as being formed in the plane of focus. As a consequence, the magnification factor of the imaging system can be ignored. After a light ray, coming from a particle in the PIV measurement plane, has left the refractive index field in the test section, it propagates along a straight line. A linear backward extension of that line to the plane of focus provides the position at which that particle is perceived by the imaging system (Fig. 1). For simplicity, it is assumed in the figures that the imaging system only collects light rays that are parallel to the optical axis after leaving the refractive index field. However, for the description of the optical errors this limitation is not essential. Figure 1 (left) shows an undisturbed light ray propagating through a homogeneous refractive index field and the disturbed one (through an inhomogeneous refractive index field) coming from a single particle and initially propagating in the same direction. A backward extension of the two light rays (dashed line) reveals that only for the disturbed light ray, the imaged position of the particle (white dot) is different from the exact position of the particle in the PIV plane (black dot). This spatial displacement is referred to as the position error. Figure 1 (right) shows a single particle (moving to

the right) at two different exposures. Due to the different position errors for the two particle positions, an error occurs in the imaged particle displacement between the two exposures, hence measured particle velocity. This is referred to as the direct velocity error.

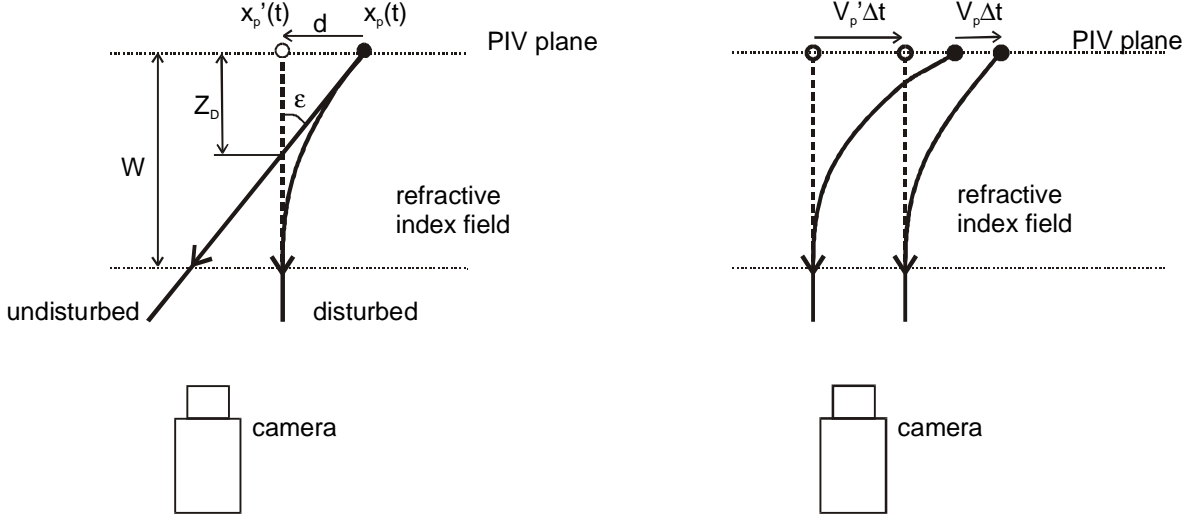


Fig. 1. Optical distortion in PIV: position error (left) and direct velocity error (right). Solid lines represent light ray trajectories coming from the particle (black dot). Dashed lines are the backward extension of those rays indicating the position where the particle appears in the PIV image (white dot).

## 2.1 Particle position error

Let the image distortion be expressed in terms of an optical displacement vector  $\vec{d}(\vec{x})$ , as:

$$\vec{d}(\vec{x}_p(t)) = \vec{x}_p'(t) - \vec{x}_p(t) \quad (1)$$

where  $\vec{x}_p(t)$  is the exact particle location  $(x,y)$  in the measurement plane and  $\vec{x}_p'(t)$  is the location where that particle is imaged (Fig. 1 left). The optical displacement vector is directly equivalent to the position error of the measurement and is related to the gradient of the refractive index  $\nabla n$ . Applying BOS theory (Richard and Raffel 2001, Elsinga et al. 2004) gives for the optical displacement vector (using  $n \approx 1$ ):

$$\vec{d}(\vec{x}) = -Z_D \vec{\epsilon}(\vec{x}) = -Z_D \int_s \nabla n(\vec{x}, z) dz \quad (2)$$

where  $z$  is the spatial coordinate along the optical axis, normal to the PIV measurement plane,  $\epsilon$  is the light beam deflection angle and  $Z_D$  is the distance parallel to the optical axis between the measurement plane and the intersection point of the disturbed ( $\nabla n \neq 0$ ) and undisturbed (in case  $\nabla n = 0$ ) light rays coming from the same particle and starting in the same direction (Fig. 1 left). A simplified expression for the optical displacement vector can be obtained (Elsinga et al. 2004) in the assumption that the gradient of refractive index is independent of  $z$  (2D flow):

$$\vec{d}(\vec{x}) = -Z_D \int_0^W \nabla n(\vec{x}) dz = -Z_D W \nabla n(\vec{x}) = -\frac{1}{2} W^2 \nabla n(\vec{x}) \quad (3)$$

where  $W$  is the length of the light path through the refractive index field in  $z$  direction (for PIV it is the distance between measurement plane and wind tunnel window). The refractive index depends on the density  $\rho$  according to the Gladstone-Dale relation, i.e.  $n = 1 + K\rho$ , in which  $K$  is the Gladstone-Dale constant ( $2.3 \cdot 10^{-4} \text{ m}^3/\text{kg}$  for air).

## 2.2 Velocity error

Following a Lagrangian approach to the tracking of a particle (image), the exact particle velocity,  $\overline{V}_p$ , is related to the particle displacement in time as:

$$\overline{V}_p(\overline{x}_p(t)) = \frac{d\overline{x}_p(t)}{dt} \quad (4)$$

In PIV the time interval between the two exposures is finite, which may introduce a difference between the instantaneous and the measured velocity (time averaging), which is neglected in the present discussion. The observed or measured particle velocity  $\overline{V}_p'$  obtained from the optically distorted images, is given by:

$$\overline{V}_p'(\overline{x}_p'(t)) = \frac{d\overline{x}_p'(t)}{dt} \quad (5)$$

The velocity error of the measurement is now defined as the difference between the measured velocity and the exact particle velocity at the location  $\overline{x}$  in the image:

$$\begin{aligned} \Delta\overline{V}_p(\overline{x}) &= \overline{V}_p'(\overline{x}) - \overline{V}_p(\overline{x}) = \left\{ \overline{V}_p'(\overline{x}_p'(t)) - \overline{V}_p(\overline{x}_p(t)) \right\} + \left\{ \overline{V}_p(\overline{x}_p(t)) - \overline{V}_p(\overline{x}_p'(t)) \right\} \\ &= \left\{ \frac{d\overline{x}_p'(t)}{dt} - \frac{d\overline{x}_p(t)}{dt} \right\} + \frac{\partial\overline{V}_p}{\partial\overline{x}}(\overline{x}_p(t) - \overline{x}_p'(t)) \end{aligned} \quad (6)$$

Substitution of the optical displacement vector (Eq. 1) and further evaluation yields:

$$\Delta\overline{V}_p(\overline{x}) = \frac{d\overline{d}(\overline{x}(t))}{dt} - \frac{\partial\overline{V}_p}{\partial\overline{x}}\overline{d}(\overline{x}) = \frac{\partial\overline{d}}{\partial\overline{x}}\overline{V}_p(\overline{x}) - \frac{\partial\overline{V}_p}{\partial\overline{x}}\overline{d}(\overline{x}) = (\nabla\overline{d})\overline{V}_p - (\nabla\overline{V}_p)\overline{d} \quad (7)$$

The first term is the direct velocity error (Fig. 1-right), which is given by the product of the exact particle velocity with the gradient of the optical displacement vector (representing a local change in optical magnification, which stretches the image length scales with respect to the physical length scales in the measurement plane). The second term in Eq. 7 is the product of the optical displacement vector with the gradient of the exact particle velocity and represents the contribution of the position error to the velocity error. It has been assumed in the analysis that in first approximation  $\nabla\overline{d}$  is constant over the particle displacement between the recordings and that the velocity gradient is constant over the optical displacement  $\overline{d}$  (first order Taylor expansion). Note that only the derivative of the optical displacement vector taken in the direction of the velocity vector contributes to the first term of the velocity error. It was shown previously that the optical displacement vector is related to the gradient of refractive index (Eq. 3). Using this result, the gradient of the optical displacement vector is given by:

$$\nabla\overline{d}(\overline{x}) = -\frac{1}{2}W^2 \frac{\partial\nabla n(\overline{x})}{\partial\overline{x}} = -\frac{1}{2}W^2 \nabla^2 n(\overline{x}) \quad (8)$$

Under certain conditions the optical displacement vector field  $\overline{d}$  can be measured independently using the BOS technique. In that case the measured velocity  $\overline{V}_p'$  can be corrected using the expression for the velocity error (Eq. 7) to obtain the exact particle velocity  $\overline{V}_p$ , as explained in the remainder.

## 2.3 Particle image blur

Figure 2 shows the principle of geometrical particle image blurring. The particle image is stretched (or compressed) due to the stretching by the inhomogeneous refractive index field (i.e. second derivative of the refractive index) of the image length scales with respect to the physical length scales in the PIV measurement plane. The principle is the same as for the direct velocity error, described above. However particle image blur becomes visible only for very large values of the optical displacement gradient. For a particle diameter of 1.0  $\mu\text{m}$  and a diffraction spot of 20.0  $\mu\text{m}$ , the imaged

particle size is expected to double in the direction of the gradient of the optical displacement vector for  $\nabla \bar{d} = 20$  pixels/pixel, causing distinct particle image blur, whereas  $\nabla \bar{d} = 0.1$  pixels/pixel introduces a 10% change of the geometrical size of the particle to  $1.1 \mu\text{m}$  resulting in an imaged particle size of  $20.1 \mu\text{m}$ , which is not directly identified as particle image blur. However in the latter case the velocity error can be as much as 10% (Eq. 7). It can therefore be concluded that significant velocity errors due to optical distortion may occur before particle image blur is visible in the PIV recordings.

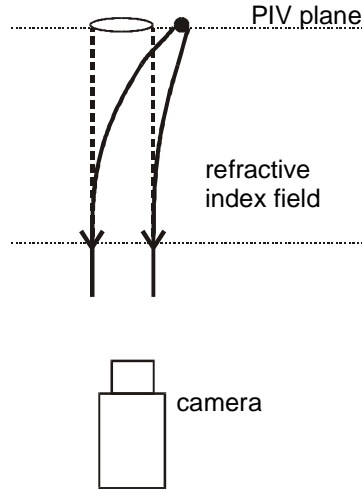


Fig. 2. Geometrical particle image blur. Solid lines represent light ray trajectories coming from the particle (black dot) edges in an inhomogeneous refractive index field. Dashed lines are the backward extension of those rays indicating the edges where the particle appears in the PIV recordings (white ellipse).

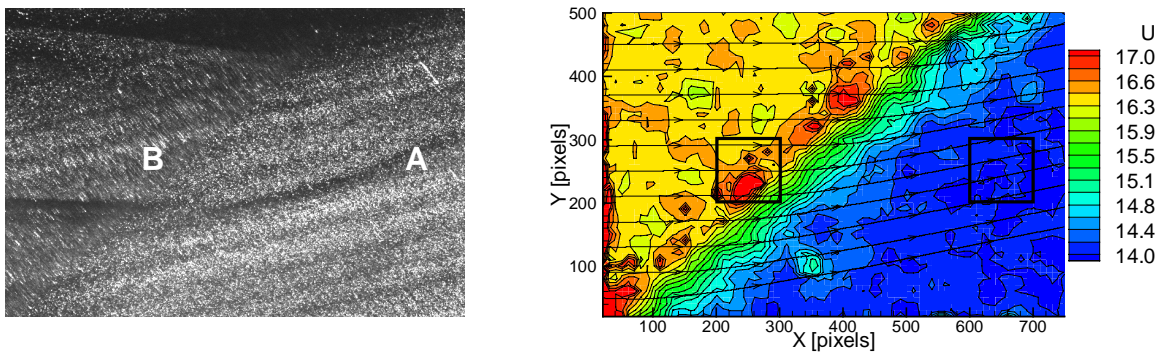


Fig. 3. PIV recording (left) of a 2D supersonic flow across an oblique shock wave and the resulting  $u$ -component of velocity in pixel units with streamlines (right). The Mach number in the uniform flow region before the shock is 2.0 and the flow deflection angle is  $11.3^\circ$ . Location (A) is in the uniform flow region behind the shock and (B) is located at the shock. (A) and (B) correspond with the squares in the right figure.

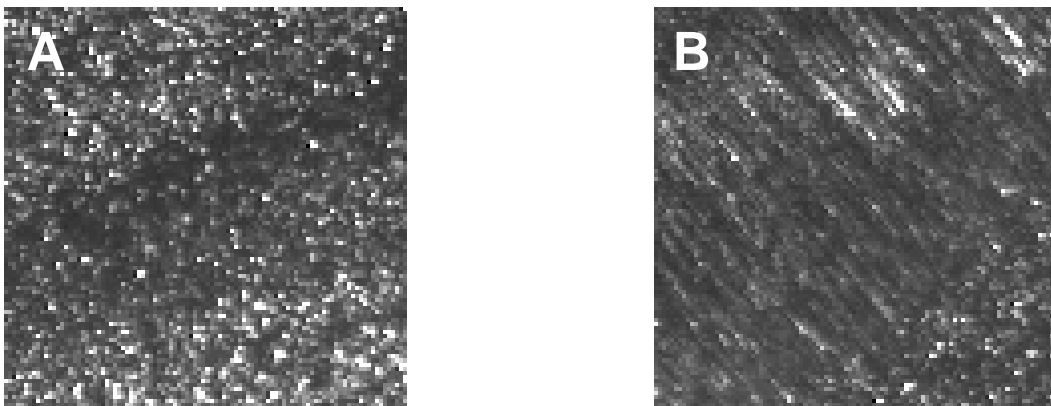


Fig. 4. Details (100x100 pixels) of the PIV recording of Fig. 3 at positions A and B.

The very large optical displacement gradient that causes particle image blur is typically encountered when measuring flow features acting as optical interfaces such as shock waves, shear layers and boundary layers. Also a focused expansion (Prandtl-Meyer expansion fan) may cause particle image blur close to the focus in some flow conditions. An example of particle image blur is given by Fig. 3, which shows a PIV image of a 2D shock wave and the measured velocity field. Details of the image at locations (A) and (B) are presented in Fig. 4. In the uniform flow region (A) the gradient of the refractive index is zero, so the particles are imaged without geometrical blur. At location (B), representing the shock wave, the particle image is blurred in the direction normal to the shock as expected due to the strong changes in the refractive index locally. It is seen in Fig. 4 that the particle brightness has decreased as a result of blur. An estimate for the enlargement  $s$  in the measurement plane near a shock wave is given by (Raffel and Kost 1998):

$$s = W\sqrt{2\Delta n} \quad (9)$$

where  $\Delta n$  is the change of the refractive index over the shock. The factor  $\sqrt{2\Delta n}$  is the maximum light deflection angle caused by the shock. For the present case the enlargement is estimated at 1.6 mm corresponding to approximately 60 pixels. This is an overestimation judging from Fig. 4, although it is difficult to determine the exact enlargement from the figure due to the low illumination intensity.

When comparing the cross-correlation results for (A) and (B), indicated in Fig. 3 (right) by the two squares, it is seen that at the location with particle image blur (B) the measurement noise has increased. This is explained by the correlation peak broadening with consequent drop in the signal to noise ratio and cross-correlation accuracy. Furthermore, particle image blur causes an increase of the flow velocity in front of the shock wave, as seen from Fig. 3 (right).

### 3. SCALING RULES FOR LARGE SCALE EXPERIMENTS

Equation 3 indicates that the optical displacement vector, hence the error in the position of a particle, increases with  $W^2$ . Therefore the problem of optical distortion increases rapidly with the dimension of the wind tunnel  $L$  or flow field size. Note that going from a small-scale research wind tunnel ( $L \sim 0.1\text{m}$ ) to industrial scale facilities ( $L \sim 1\text{m}$ ) easily involves a scale factor for  $L^2$ , hence  $W^2$ , of the order of 100. However, generally the model dimensions and the flow features associated to the inviscid flow behaviour scale linearly with the wind tunnel size. As a consequence also with the field of view is linearly increased. Viscous flow features are expected to scale less than linear, with  $L^{0.5}$  for laminar flow and  $L^{0.8}$  for turbulent flow (White 1991). Therefore it is expected that  $\nabla n$  decreases with  $L^{-0.5}$  or  $L^{-0.8}$  (given a certain density level of the flow) and that  $\nabla^2 n$  decreases with  $L^{-1}$  or  $L^{-1.6}$  for laminar and turbulent flow respectively. In conclusion, it is estimated that the position error in meters (Eq. 3) scales at most as  $L^{1.5}$ , or in pixel units as  $L^{0.5}$ . The direct velocity error in m/s (Eq. 7) scales at most as  $L$ .

At optical interfaces, i.e. shock waves, the refractive index is discontinuous (or its derivatives vary strongly with  $\bar{x}$ ) and therefore Eq. 3 and 7 do not hold. In the vicinity of the interface strong particle image blur is expected accompanied by a velocity error. The extent for the particle image blur scales as  $W$ , hence  $L$ , as is shown by Eq. 9. In pixel units the enlargement is independent of  $L$ .

### 4. CORRECTING OPTICAL DISTORTION USING BOS

The BOS method uses the optical distortion effects to measure the refractive index field (Raffel et al. 2000, Richard and Raffel 2001, Klinge and Riethmuller 2002, Elsinga et al. 2004). The BOS technique is very similar to PIV. It employs a computer generated PIV image, which in the present study is placed at the back of the test section. The background pattern is imaged with a high-resolution CCD camera before and during the experiment. Thus two images of the background pattern are taken and the relative displacement caused by the difference in the refractive index field is measured by means of cross-correlation similarly to what is performed in PIV.

In BOS, the undistorted pattern is known from a recording of the background without flow in the test section (homogeneous refractive index), whereas in PIV both recordings are distorted, and the particle displacement cannot be distinguished from the optical distortion. The displacement field measured independently with BOS can be used to correct PIV measurements. However, the BOS displacement vector is obtained with the particle image pattern placed on the opposite side of the wind tunnel, whereas the PIV measurement plane is located inside the flow, often in the mid-section. The BOS displacement vector to be applied for correction of the PIV measurements requires therefore a

proper scaling, since the gradient of refractive index is integrated over different paths:  $W_{BOS}$  and  $W_{PIV}$ . To obtain the scaling factor it is assumed that the light rays collected by the imaging optics are parallel to the optical axis for both BOS and PIV, so that the field of view of BOS does not need to be scaled to the field of view in the PIV measurement plane (Klinge and Riethmuller 2002). When assuming that the gradient of refractive index is independent of  $z$  (2D flow), the optical displacement vector due to the refractive index field in BOS  $\vec{d}_{BOS}$  and PIV  $\vec{d}_{PIV}$  are given by:

$$\begin{aligned}\vec{d}_{BOS}(\vec{x}) &= -(Z_D W)_{BOS} \nabla n(\vec{x}) \\ \vec{d}_{PIV}(\vec{x}) &= -(Z_D W)_{PIV} \nabla n(\vec{x})\end{aligned}\quad (10)$$

Substitution of the gradient of the refractive index yields:

$$\vec{d}_{PIV}(\vec{x}) = \frac{(Z_D W)_{PIV}}{(Z_D W)_{BOS}} \vec{d}_{BOS}(\vec{x}) = A \vec{d}_{BOS}(\vec{x}) \quad (11)$$

where  $A$  is the scaling factor. With  $Z_D=W/2$  and with the PIV measurement plane located at the center of the test section ( $W_{PIV}=W_{BOS}/2$ ) then  $A=1/4$ . Using  $\vec{d}_{PIV}$  with Eq. 1 and the first right-hand-side term of Eq. 7 for the direct velocity error (the second term has the same effect as using Eq. 1 to correct for the measurement position), the PIV measurement can be corrected for optical distortion by applying:

$$\begin{aligned}\vec{x}_{P\ corr} &= \vec{x}_P - \vec{d}_{PIV} \\ \vec{V}_{P\ corr}(\vec{x}_{P\ corr}) &= \left( I + \nabla \vec{d}_{PIV} \right)^{-1} \vec{V}_P(\vec{x}_{P\ corr})\end{aligned}\quad (12)$$

where  $I$  is the identity matrix. For more complex flow configurations (axi-symmetric or 3D) finding the scaling rule is more difficult or may even be impossible, because the variation of the gradient of refractive index with  $z$  is unknown.

## 5. SIMULATION

The model for the position and velocity error due to optical distortion, as presented in a previous section, is evaluated with numerical simulation of PIV experiments in the presence of an inhomogeneous refractive index field. Seeding, flow, illumination and imaging conditions are simulated taking as a reference actual experimental conditions in the transonic-supersonic wind tunnel (TST-27) at the Aerodynamics Laboratories of the Delft University of Technology. Seeding particles with a relaxation time  $\tau_p=2.4\mu s$  are traced through a 2D flow field. The optical distortion is calculated using a light ray-tracing algorithm in the refractive index field. Using the results from particle and ray traces, synthetic PIV recordings are produced, which are analyzed using a window deformation iterative multi-grid scheme (WIDIM, Scarano and Riethmuller 2000) with interrogation windows of  $31 \times 31$  pixels and 50% overlap. The PIV recordings are separated in time by  $1\mu s$ . Furthermore synthetic BOS images are generated in order to demonstrate the effectiveness of the BOS correction method for 2D flows. The dimensions of the test section and setup are  $W_{PIV}=140\text{mm}$ ,  $W_{BOS}=280\text{mm}$ ,  $Z_{D\_PIV}=W_{PIV}/2$  and  $Z_{D\_BOS}=164\text{mm}$  (taking into account the effect of the rear window). Consequently the scaling factor  $A$  is equal to 0.21.

Two types of flow with non zero velocity only in the horizontal direction ( $v=0$ ) are considered: a one-dimensional expansion front and a shear layer of constant thickness, which are simplified models of realistic compressible flow features, such as (Prandtl-Meyer) expansion fan and a shear layer with increasing thickness in flow direction, which will be considered in the experimental verification (section 6). The simplifications allow identifying the effects of the position error and the direct velocity error separately.

### 5.1 Shear layer

The flow velocity  $u$  across a shear layer is modeled as:

$$u(y) = u_0 + \Delta u \tanh\left(\frac{y}{\delta_o}\right) ; \quad \delta_o = \frac{\Delta u}{\left(\frac{du}{dy}\right)_{y=0}} \quad (13)$$

where  $\Delta u=250\text{m/s}$  ,  $u_o=250\text{m/s}$  and  $\delta_o=3\text{mm}$  is a thickness parameter. The velocity above and below the shear layer is  $500\text{m/s}$  and  $0$  respectively. Because the flow acceleration is zero the tracer particles travel at the flow velocity. Given a density of  $0.90\text{kg/m}^3$  above the shear layer and assuming constant total temperature ( $290\text{K}$ ) and pressure across the shear layer, the density below the shear layer is  $0.51\text{kg/m}^3$ . The refractive index field is found using the Gladstone-Dale relation. Since the refractive index is a function of the  $y$ -coordinate only, the gradient of the optical displacement vector (oriented in  $y$  direction, Eq. 8) is perpendicular to the velocity vector (oriented in  $x$  direction). Therefore the first term of the velocity error (direct velocity error, Eq. 7) cancels out and only the position error remains. Substituting Eq. 3 and the Gladstone-dale relation, the resulting velocity error for the shear layer is given by:

$$\Delta u(y) = -\frac{\partial u(y)}{\partial y} d_y(y) = \frac{W^2}{2} K \frac{\partial \rho(y)}{\partial y} \frac{\partial u(y)}{\partial y} \quad (14)$$

where  $d_y$  is the  $y$ -component of the optical displacement vector.

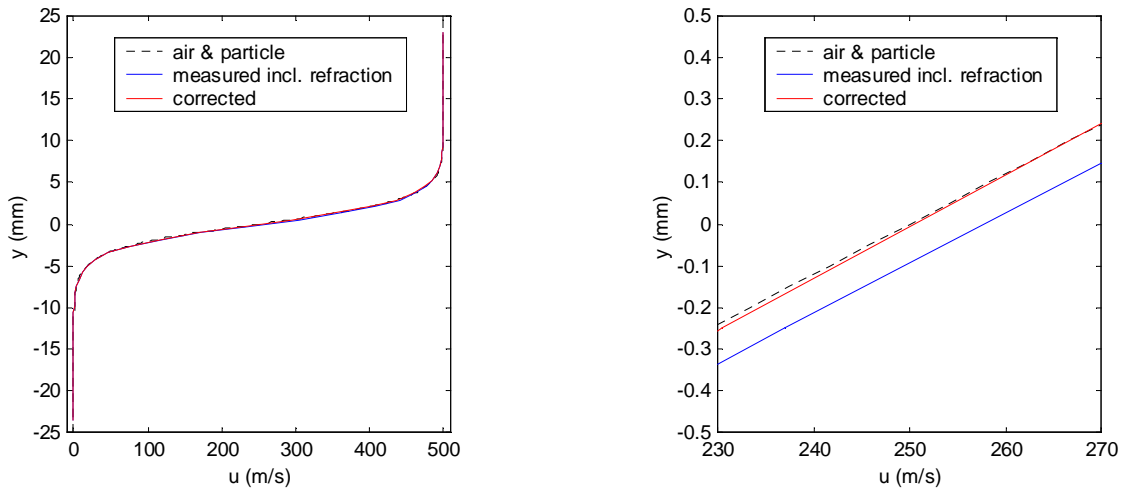


Fig. 5. Velocity profiles across the shear layer (left) and detail (right) with  $\delta_o=3\text{mm}$

Figure 5 shows the velocity profile across the shear layer. The qualitative agreement between measured and flow velocity is good. The error due the refractive index fields can be appreciated in a close-up (Fig. 5 right). The position error is  $0.094\text{mm}$  or  $1.9$  pixels, which is not detectable on the scale of the field of view ( $50\text{mm}$ ). Due to the large velocity gradient in the shear layer the velocity error at  $y=0$  is more significant:  $7.9\text{m/s}$ . Using the BOS correction the error reduces by  $93\%$  to  $0.6\text{m/s}$  (corresponding to  $0.01$  pixel particle displacement).

Changing the thickness of the shear layer  $\delta_o$  does not yield significantly different results. The range of  $\delta_o$  on which the presented optical distortion model and the BOS correction method are effective is limited on the one end by insufficient resolution for cross-correlation resulting in amplitude modulation ( $\delta_o=1\text{mm}$ , cross-correlation errors dominate) and on the other end by the cross-correlation accuracy ( $\delta_o=5\text{mm}$ , the error associated with optical distortion is smaller than the cross-correlation accuracy).

## 5.2 One-dimensional compression/expansion front

The flow velocity  $u$  in horizontal direction is taken as:

$$u(x) = u_o + \Delta u \tanh\left(\frac{x}{\delta_o}\right) \quad (15)$$

where  $\Delta u=35\text{m/s}$  ,  $u_o=465\text{m/s}$  and  $\delta_o=3\text{mm}$ . The velocity before and behind the expansion is  $430\text{m/s}$  and  $500\text{m/s}$  respectively. Given a density of  $0.90\text{kg/m}^3$  before the expansion, a total temperature of  $290\text{K}$  and using isentropic flow relations, the density behind the expansion is  $0.58\text{kg/m}^3$ . In this case, the refractive index is a function of  $x$  only. Therefore the gradient of the optical displacement vector (Eq. 8) is oriented in the direction of the velocity vector ( $x$

direction) and both position and direct velocity errors are to be expected. The velocity error for the one-dimensional expansion is given by:

$$\Delta u(x) = \frac{\partial d_x(x)}{\partial x} u(x) - \frac{\partial u(x)}{\partial x} d_x(x) = \frac{W^2}{2} K \left[ -\frac{\partial^2 \rho(x)}{\partial x^2} u(x) + \frac{\partial \rho(x)}{\partial x} \frac{\partial u(x)}{\partial x} \right] \quad (16)$$

where  $d_x$  is the  $x$ -component of the optical displacement vector. The second term of the velocity error is similar to the velocity error for the shear layer (Eq. 14).

Figure 6 shows the velocity profile across the expansion. Particle lag is clearly seen as a shift of the profile in the flow direction of about 1mm leading to a velocity error of -10m/s at  $x=0$ mm. Since the flow velocity cannot be measured more accurately than the particle velocity, the error due to optical distortion is defined with respect to the particle velocity. The refractive index field has a large effect on the measured velocity profile, as seen from Fig. 6. Not only a velocity error is introduced, but also the shape of the velocity profile has changed dramatically, which may lead to a misinterpretation of the flow. The most important source of error is the first term in Eq. 7, which represents the stretching of the image length scales with respect to the physical length scales in the PIV measurement plane due to the gradient of the optical displacement vector. As also seen from the results of the shear layer, the error directly related to the optical displacement vector does not result in a significant change in the shape of the velocity profile. In conclusion: even though the shear layer and the expansion have approximately the same thickness and density level, the velocity errors are very different due to the different orientation of the optical distortion with respect to the velocity vector, leading to the absence or presence of the direct velocity error.

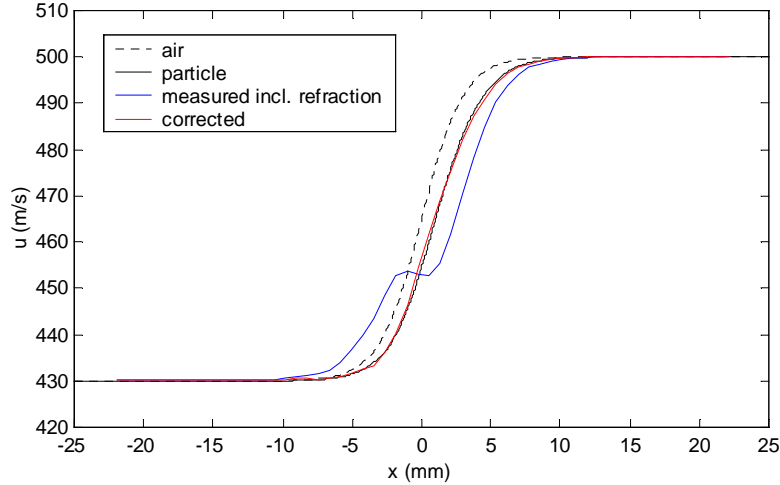


Fig. 6. Velocity profiles across the one-dimensional expansion with  $\delta_0=3\text{mm}$

The maximum error in position is 0.12 mm (2.4 pixels). The largest error in velocity is -14m/s (found at  $x=2\text{mm}$ ), which for 95% is due to the gradient of the optical displacement vector. Using the BOS correction the error reduces with 95% to -0.74m/s (corresponding to 0.15 pixel particle displacement).

Increasing the expansion thickness  $\delta_0$  to 5mm, thereby reducing the optical distortion effects, results in a less profound change in the shape of the measured velocity profile (Fig. 7): the wiggle as seen in Fig. 6 has disappeared. However the velocity gradient is clearly underestimated by PIV. From Fig. 7 it is again seen that the BOS can be used effectively to correct for optical distortion. Concerning the range of  $\delta_0$  on which the optical distortion model and the BOS correction method are effective, the same considerations hold as for the shear layer.

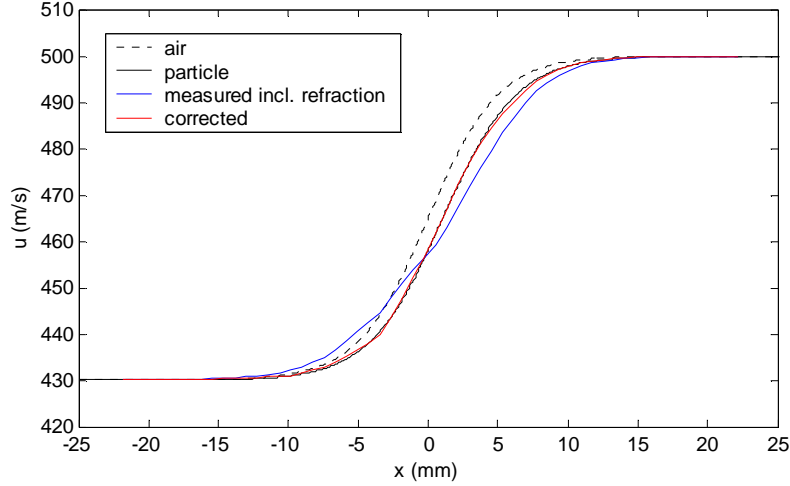


Fig. 7. Velocity profiles across the one-dimensional expansion with  $\delta_0=5\text{mm}$

## 6. EXPERIMENTS

In this section experimental evidence of the velocity error due to optical distortion in compressible flow is given. In absence of true particle velocity data the errors are evaluated and corrected for using the BOS method. The results are compared with the trends seen in the simulations.

The flow around the 2D wedge-plate model (Fig. 8) is measured in the TST-27 supersonic wind tunnel at  $M_\infty=1.96$  and  $P_0=1.97$  bars. The model spans the width of the test section (280 mm) and consists of a wedge with sharp leading edge imposing a flow deflection of  $11.31^\circ$ , followed by a plate 50mm long and 20mm thick. Figure 8 visualizes the following flow features: the bow shock (blue) followed by two expansions (marked green on the upper surface) and separated flow at the base resulting in the formation of shear layers (blue). The shear layers from both corners reattach thereby enclose the recirculation region. At reattachment the streamlines are concave causing a recompression to be formed. For the experimental investigation only the expansion fan located at the model shoulder and the shear layer are considered. The experimental parameters are the same as for the simulation (section 5).

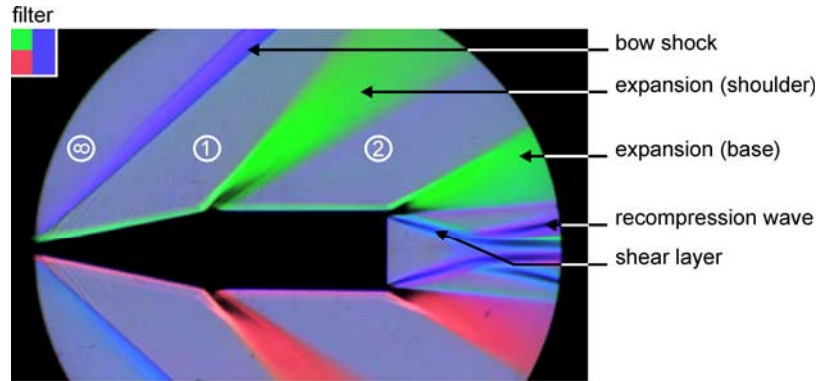


Fig. 8. Schlieren image of the flow around the 2D wedge-plate model,  $M_\infty=2$

In the real PIV and BOS experiments the light collected by the imaging optics is not parallel as was the case in the simulations. This means that the density gradient is not constant along the optical path everywhere in the field of view. However in the center of the field of view the viewing angle with respect to the optical axis is small, so the density gradient can be assumed constant and BOS can be used to quantify the optical distortion effects in PIV. Therefore the image center is positioned close to the flow features of interest. Furthermore in non-parallel imaging the BOS field of view needs to be scaled to the field of view in the PIV measurement plane (Klinge and Riethmuller 2002). Between PIV and BOS measurements the camera position remains fixed and only the focus is changed to a different plane. This way the field of view in the PIV measurement plane, which is  $55 \times 44 \text{mm}^2$  for all experiments, does not change. The image resolution is  $1280 \times 1024$  pixels.

### 6.1 Shear layer

Figure 9 left shows the measured  $u$ -component of velocity in the separated wake flow averaged over 160 instantaneous velocity fields. In order to compare the measurement results with the simulation, the velocity in the direction of the shear layer  $V_s$  (in the direction of  $s$ , Fig. 9 left) is evaluated. Normal to the shear layer (in the direction of  $r$ , Fig. 9 left) the velocity is negligible. Figure 9 right presents a cross-plot of  $V_s$  along  $r$ . It is seen that the velocity across the shear layer ranges from 520m/s to  $-50$ m/s. Using the free stream conditions, shock relations, Prandtl-Meyer theory and assuming constant pressure and total temperature across the shear layer, the density above and below the shear layer is estimated at  $0.61\text{kg/m}^3$  and  $0.31\text{kg/m}^3$  respectively. As expected from the simulation of the shear layer (section 5.1) the measurement overestimates the local velocity. At  $r=0$  the BOS measurement predicts a velocity error of 5.8 m/s (corresponding to 0.14 pixel particle displacement) with a position error of 0.040mm, for which the measurement is corrected (Fig. 9 right). The magnitude of the correction agrees well with the simulation results, taking into account that the overall density level in the measurement, hence density gradient, is 67% of that used in the simulation.

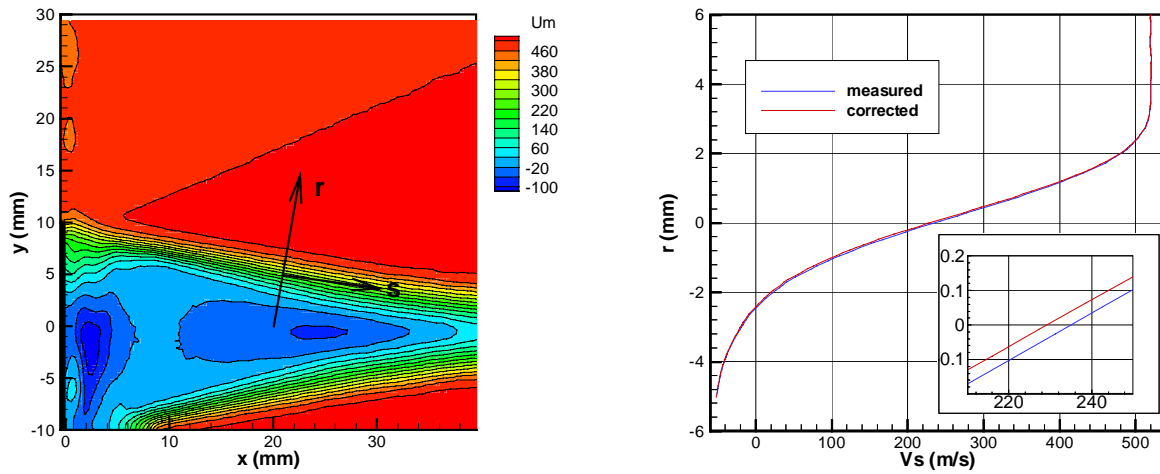


Fig. 9. Measured  $u$ -component of velocity in the base region of the 2D wedge-plate model (left), and a cross-plot in the direction normal to the shear layer of the measured and corrected flow velocity  $V_s$  in the direction of the shear layer (right)

### 6.2 Prandtl-Meyer expansion fan

The measurement result for the Prandtl-Meyer expansion fan located at the model shoulder is shown in Fig. 10 left. The average velocity field is composed from 165 instantaneous fields. For good comparison with the simulation of a one-dimensional expansion (section 5.2) the velocity component in the direction of the density gradient  $V_s$  (in the direction of  $s$ , Fig. 10 left) is considered here. Figure 10 right presents a cross-plot of  $V_s$  along  $s$ .  $V_s$  increases from 232m/s to 335m/s over the expansion. Using the free stream conditions, shock relations and Prandtl-Meyer theory, the density before and after the expansion is  $0.92\text{kg/m}^3$  and  $0.61\text{kg/m}^3$  respectively. The measured and BOS corrected velocity profile resemble the simulation results of Fig. 7. The PIV measurement underestimates the velocity gradient inside the expansion. Furthermore the measurement displays a region of increased velocity just before the expansion, which largely disappears after the measurement has been corrected using BOS. At  $s=2.5\text{mm}$  the velocity error is  $-6.5\text{m/s}$  (corresponding to 0.15 pixel particle displacement). Compared to the simulation the velocity error is smaller, because the velocity in the direction of the density gradient  $V_s$  is also smaller.

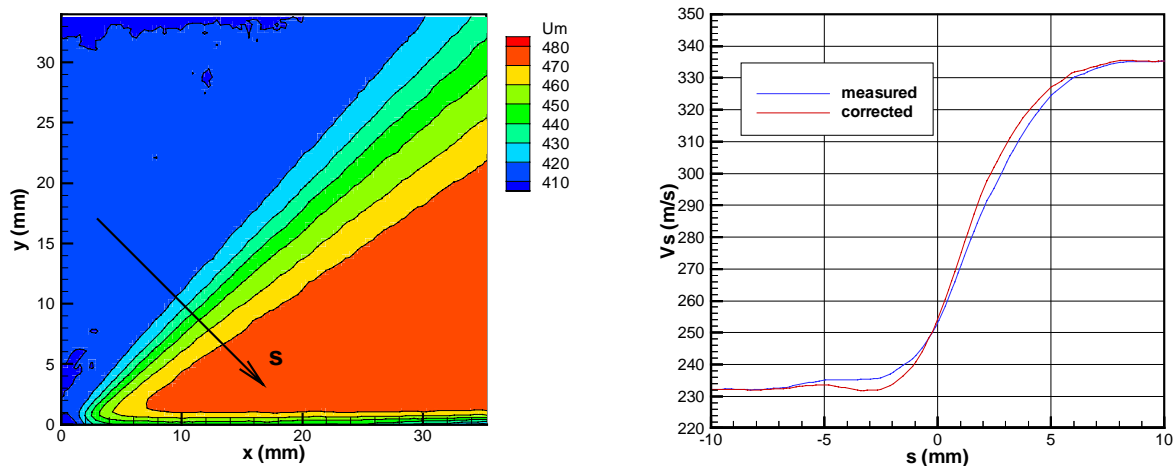


Fig. 10. Measured  $u$ -component of velocity in the expansion located at the shoulder of the 2D wedge-plate model (left), and a cross-plot in the direction normal to the Mach waves of the measured and corrected flow velocity  $V_s$  in this direction (right)

## 7. CONCLUSIONS

Three types of error affecting PIV measurements in optically inhomogeneous media were identified. The position error and the velocity error are directly related to the overall systematic error on the velocity measurement and are caused by the gradient and the second derivative of the refractive index respectively. The particle image blur, which is related to the second derivative of the refractive index, introduces a correlation peak broadening with consequent drop in the signal to noise ratio. It was shown that the presence of particle image blur indicates already that the measurement is seriously affected by the velocity error.

Evidence of these forms of error was presented by means of PIV recordings obtained in supersonic flow. Moreover the effects were quantified with a numerical simulation of particle motion, illumination and imaging through compressible flow. Two simple test flows were used for the simulation: a shear layer and a one-dimensional expansion. The tests demonstrated that the second derivative of the refractive index in the direction of the velocity vector is the major source for the velocity error. The position error was generally of the order of 2 pixels, which is difficult to appreciate on the scale of the complete field of view. Moreover it is concluded that investigating shearing interfaces is much less critical in comparison with compression/expansion fronts. An experimental assessment of a shear layer and a Prandtl-Meyer expansion flow in the supersonic wind tunnel confirmed the results of the simulation. Furthermore it was demonstrated that PIV application to large-scale compressible flows could suffer from very large optical distortion errors on the velocity.

A correction procedure for the position and velocity error was shown to be possible for 2D flows. The distortion effects due to the refractive index field were measured independently with BOS and applied to correct the PIV measurement. Based on the results from the simulated experiments, the BOS correction reduced the velocity error up to 95%.

## REFERENCES

- Elsinga GE, van Oudheusden BW, Scarano F, Watt DW (2004) Assessment and application of quantitative schlieren methods: Calibrated color schlieren and background oriented schlieren. *Exp Fluids* 36: 309-325
- Haertig J, Havermann M, Rey C and George A (2002) Particle image velocimetry in Mach 3.5 and 4.5 shock-tunnel flows. *AIAA J* 40: 1056-1060
- Klinge F, Riethmuller ML (2002) Local density information obtained by means of the Background Oriented Schlieren (BOS) method. *11th international symposium on application of laser technology to fluid mechanics*, Lisbon, Portugal, paper 15.3

- Raffel M, Kost F (1998) Investigation of aerodynamic effects of coolant ejection at the trailing edge of a turbine blade model by PIV and pressure measurements. *Exp Fluids* 24: 447-461
- Raffel M, Richard H, Meier GEA (2000) On the applicability of background oriented optical tomography for large scale aerodynamic investigations. *Exp Fluids* 28:477-481
- Richard H, Raffel M (2001) Principle and applications of the background oriented schlieren (BOS) method. *Meas Sci Technol* 12:1576-1585
- Scarano F, Riethmuller ML (2000) Advances in iterative multigrid PIV image processing. *Exp Fluids* 29, S051
- Scarano F, Van Oudheusden BW (2003) Planar velocity measurements of a two-dimensional compressible wake. *Exp Fluids* 34: 430-441
- Urban WD, Mungal MG (2001) Planar velocity measurements in compressible mixing layers. *J Fluid Mech* 431: 189-222
- White FM (1991) *Viscous fluid flow*. McGraw-Hill, New York